Effect of cell geometry in the evaluation of erythrocyte viscoelastic properties

Fran Gómez,[1,2,5] Leandro S. Silva,[3] Glauber Ribeiro de Sousa Araújo,[3] Susana Frases,[3] Ana Acacia S. Pinheiro,[3] Ubirajara Agero,[4] Bruno Pontes,[1,2,5] and Nathan Bessa Viana[1,2,5,*]

[1]*Instituto de Física, Universidade Federal do Rio de Janeiro, Rio de Janeiro, Rio de Janeiro, 21941-972, Brazil*

[2]*LPO-COPEA, Instituto de Ciências Biomédicas, Universidade Federal do Rio de Janeiro, Rio de Janeiro, Rio de Janeiro, 21941-902, Brazil*

[3]*Instituto de Biofísica Carlos Chagas Filho, Rio de Janeiro, Rio de Janeiro, 21941-901, Brazil*

[4]*Instituto de Ciências Exatas, Departamento de Física, Universidade Federal de Minas Gerais, Belo Horizonte, Minas Gerais, 31270-901, Brazil*

[5]*CENABIO - Centro Nacional de Biologia Estrutural e Bioimagem, Universidade Federal do Rio de Janeiro, Rio de Janeiro, Rio de Janeiro, 21941-902, Brazil*

(Received 18 September 2019; revised manuscript received 20 April 2020; accepted 11 May 2020; published 2 June 2020)

The red blood cell membrane-cytoskeleton is a complex structure mainly responsible for giving the cell rigidity and shape. It also provides the erythrocyte with the ability to pass through narrow capillaries of the vertebrate blood circulatory system. Although the red blood cell viscoelastic properties have been extensively studied, reported experimental data differ by up to three orders of magnitude. This could be attributed to the natural cell variability, to the different techniques employed, and also to the models used for the cell response, which are highly dependent on cell geometry. Here, we use two methodologies based on optical tweezers to investigate the viscoelastic behavior of healthy human red blood cells, one applying small cell deformations (microrheology) and another imposing large deformations (tether extraction). We also establish a defocusing microscopy-based method to characterize the cell geometry and thus the erythrocyte form factor, an essential parameter that allows comparisons among the viscoelastic properties at different conditions. Moreover, for small deformations, a soft glassy rheology model is used to discuss the results, while for large deformations two surface shear moduli and one surface viscosity are determined, together with the surface tension and bending modulus of the erythrocyte membrane lipid component. We also show that F-actin is not detected in tethers, although the erythrocyte membrane has physical properties like those of other adherent cells, known to have tethers containing F-actin inside. Altogether, our results show good agreement with the reported literature and we argue that, to properly compare the viscoelastic properties of red blood cells in different situations, the task of cell geometry characterization must be accomplished. This may be especially important when the influence of agents, like the malaria parasite, induces changes in both the geometry and chemical constituents of the erythrocyte membrane. Together, the new methodologies and procedures used in this study would allow the erythrocyte community to better explore the mechanical behavior of red blood cells and may be useful to characterize erythrocyte viscoelasticity changes in several blood diseases.

DOI: 10.1103/PhysRevE.101.062403

I. INTRODUCTION

Mature human red blood cells (RBCs) are extremely differentiated and play a vital role in the respiratory system, transporting gas to the cells from all tissues through the whole body. The absence of a nucleus and other inner membrane organelles along with a flexible membrane structure are features that allow the RBCs to undergo large deformations and to go through all blood vessels, including very narrow capillaries that sometimes have smaller diameters than the RBC typical length [1]. The huge amount of hemoglobin molecules in the RBC is critical for oxygen transportation. However, this molecule is also the most important source of amino acids used by the malaria parasite *Plasmodium* spp. during its replicative cycle inside RBCs [2]. All along its development, the parasite induces dramatic mechanical changes on the RBCs. The most remarkable ones are the increase of stiffness and reduction of membrane flexibility, both being highly associated with malaria pathogenesis. It is well known that microvascular congestion and sequestration of infected RBCs in vital organs, such as the brain and lung, are related to the most severe malaria cases, especially when induced by the most virulent human malaria parasite, the *Plasmodium falciparum* [3]. Better comprehension of how the RBC mechanical properties change during the *Plasmodium falciparum* erythrocytic cycle could help to develop new therapeutic strategies to reduce the most severe cases related to microvascular congestion and sequestration of infected RBCs.

The linear elastic response of an isotropic material is characterized by two independent parameters: the compression modulus K_V and the shear modulus G [4]. Two other parameters widely used in elasticity theory are the material Young's modulus Y and its Poisson's ratio σ_p. Y and σ_p are

*Corresponding author: nathan@if.ufrj.br

described as functions of K_V and G, and for many materials, $\sigma_p = 1/3$ and only the shear modulus is used to characterize the material response, once $K_V = Y = 8G/3$ in this situation [4]. On the other hand, the linear viscous response of an isotropic Newtonian liquid is also characterized by only one parameter, the viscosity η, which is defined as the proportionality constant between the shear stress and shear strain rate in the material.

The red blood cell membrane-cytoskeleton complex, or simply the RBC membrane, is composed mainly of a lipid bilayer associated with an underlying spectrin network, formed by tetramers of about 200 nm in length. This network gives the RBC not only its unique resistance to stress but also allows it to deform and pass through the smallest capillaries of the vertebrate circulatory system [5]. The RBC membrane is a viscoelastic material, presenting both elastic and viscous behaviors. Isotropic viscoelastic materials are characterized by their complex shear modulus $G^*(\omega) = G'(\omega) + iG''(\omega)$, where ω is the angular frequency of the stress and strain in the material. For $\omega \to 0$, $G'(\omega \to 0) = G$ and $G''(\omega \to 0)/\omega = \eta$ [4]. G' is the storage modulus and G'' is the loss modulus of the material.

The RBC membrane has an average thickness of $\zeta \approx 90$ nm and length in the micrometer scale [6]. Thus, it can be considered as a two-dimensional material with elastic response described by two parameters, the area compression modulus K_A and the surface shear modulus μ. Its viscous response is characterized by a surface viscosity η_S, a quantity that relates shear stresses and strain rates on the membrane surface. The relations between surface and bulk viscoelastic parameters are obtained by multiplying the bulk parameters by the membrane thickness [7], so that $K_A = K_V\zeta$, $\mu = G\zeta$, and $\eta_S = \eta\zeta$. Besides, considering that the RBC membrane has a Poisson's ratio $\sigma_P = 1/3$, its elastic response is only characterized by $\mu = K_A/2$ [4].

Since the pioneering work of Evans *et al.* [8], the RBC elastic (μ) and viscous (η_S) behaviors have been characterized using different techniques. Using micropipette aspiration, values of the RBC membrane surface shear modulus were obtained in the range of 1–10 pN/μm [9,10]. With the analysis of membrane thermal fluctuations [11], much higher values were obtained, $\mu \approx 1000$ pN/μm, and by measuring the local amplitude of membrane flickering a much smaller value ($\mu \approx 0$) was used to explain the results. The surface viscosity also varies among published results in the range of 0.7–9 pN s/μm [12–14], possibly due to variations in the surface shear modulus, since the most employed technique assumes that $\eta_S = \mu t_c$ [15], where t_c is the RBC relaxation time after being stretched and released to return to its relaxed form.

For the complex shear modulus $G^*(\omega)$, few reported results can be found in the literature. Using dynamic light scattering, values of the RBC storage and loss moduli were reported in the range of 0.01–1 Pa, for linear frequencies, $f = \omega/(2\pi)$, varying between 1 Hz $< f <$ 100 Hz [16]. The above results were compared to the apparent complex elastic modulus $g^*(\omega)$ obtained by optical magnetic twisting cytometry, multiplying the results in Ref. [17] by a factor of 84. The authors used this multiplicative factor for comparison purposes and claimed that it was employed to convert two-dimensional (2D) in-plane shear modulus into three-dimensional (3D) shear modulus. Furthermore, the complex shear modulus and the apparent elastic modulus for the RBC membrane-cytoskeleton complex were reported as obeying a power law in frequency with exponent $\alpha \approx 0.6$. A precise definition for the form factor F_f that relates forces and deformations to stresses and strains in the RBC membrane is needed to possibly clarify the causes for the observed discrepancies.

Optical tweezers (OT) techniques are tools used to exert forces on the scale of pN (1 pN $= 10^{-12}$ N), and to measure deformations of the order of μm. They are versatile and relatively low-cost instruments that enable single-cell experiments, and thus are suitable for investigating the cell mechanical properties. The RBC elastic constants and viscosity parameters measured by optical tweezers are not only related to biochemical alterations in the membrane but also with the cell geometry. In this work, we characterized the erythrocyte morphology by using defocusing microscopy to get the RBC height profile [18] and thus the cell form factor. The form factor was used to discuss the obtained results.

With OT-based microrheology experiments [19], we determined the complex shear modulus of the RBC membrane as a function of the angular frequency of an external load. We found that the RBC membrane rheology can be well described by a soft glassy material model, with a power law dependence of the complex shear modulus with the load angular frequency. Besides the power law exponent, the proposed phenomenological model is characterized by two shear moduli and one low-frequency viscosity, all demanding information about the cell geometry to be correctly evaluated.

With OT-based tether extraction experiments [20], we analyzed the RBC membrane viscoelasticity by measuring two surface shear moduli and one surface viscosity parameter. Moreover, we also determined the surface tension and bending modulus for the lipid component of the RBC membrane. Confocal microscopy was used to evaluate the presence of F-actin inside tethers and scanning electron microscopy to measure the tether radius. We showed that F-actin was not detected in tethers although the erythrocyte membrane has physical properties similar to those of adherent cells, known to have tethers containing F-actin inside.

In summary, we show that the cell geometry must be considered in order to properly evaluate the RBC membrane viscoelastic properties. This can be especially important when the influence of agents, like the malaria parasite, alters both geometry and chemical constituents of the RBC membrane.

II. THE RED BLOOD CELL FORM FACTOR

In order to determine the relationship between the RBC complex elastic constant $K^*(\omega)$ and its complex shear modulus $G^*(\omega)$, the defocusing microscopy was considered to characterize the RBC height profile and to determine the membrane perimeter as a function of the position in the direction of force application in the cell. As described in Ref. [18], defocusing microscopy is a bright-field microscopy technique sensitive to the light phase in the sample.

To identify the influence of the material geometry characterized by the form factor in rheology experiments consider, for instance, a block of Young's modulus Y. Supposing now

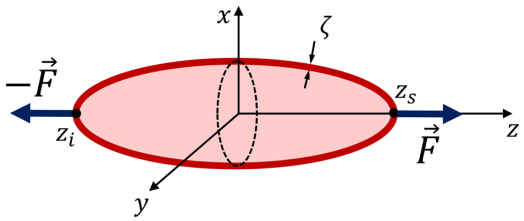

FIG. 1. Representation of the deformed RBC when subjected to a pair of forces with magnitude F. ζ is the membrane thickness, and z_s and z_i correspond to the cell limits in the z direction.

that this material has a cross section area A and length l, when it is subjected to a pair of opposed forces, with magnitude F, its length increases by a value Δl, and the following relationship can be written:

$$F = Y\left(\frac{A}{l}\right)\Delta l. \tag{1}$$

This is the expression for Hooke's law with an elastic constant $k = Y(A/L)$ that depends on the material elasticity parameter (Y), and also on its geometry (form factor defined as A/l, for this case). The defocusing microscopy has been used to study adherent cells and erythrocytes in a series of published works [21–24], one reason why it is employed here to characterize the RBC morphology.

When the RBC is subjected to a pair of forces with magnitude F (see Fig. 1), the cell deformation δ in the z direction can be determined assuming that the RBC is composed by a set of cylindrical shells associated in series, such that each one has length dz and area $p(z)\zeta$, with $p(z)$ being the perimeter of the RBC height profile obtained by the intersection of the RBC membrane with the plane z, and ζ being the membrane thickness. So,

$$\delta = \frac{F}{\zeta Y}\int_{z_i}^{z_s}\frac{dz}{p(z)}, \tag{2}$$

where Y is the Young's modulus of the RBC membrane, treated as a bulk material. z_s and z_i correspond to the cell limits in z direction.

The RBC height profile obtained applying the defocusing microscopy technique is then used to evaluate the integral described in Eq. (2), which we associate with the inverse of the form factor F_f:

$$F_f = \left(\int_{z_i}^{z_s}\frac{dz}{p(z)}\right)^{-1}, \tag{3}$$

and hence

$$F = Y\zeta F_f\delta = k_{RBC}\delta, \tag{4}$$

where $k_{RBC} = Y\zeta F_f$ is the elastic constant of the RBC. The relation between the complex elastic constant and the shear modulus is found using the corresponding principle in rheology [25], which states that the rheological response is obtained by substituting the elastic shear modulus by the complex shear modulus in the equation relating the Fourier transform of force $\tilde{F}(\omega)$ and displacement $\tilde{\delta}(\omega)$, that is,

$$\tilde{F}(\omega) = K^*(\omega)\tilde{\delta}(\omega). \tag{5}$$

For a material with Young's modulus Y and Poisson's ratio $\sigma_P = 1/3$, Y and G are related by $Y = 8G/3$ [4]. Replacing Y in Eq. (4) by $8G/3$, and G by $G^*(\omega)$ after taking the Fourier transform of E. (4), we get

$$K^*(\omega) = \tfrac{8}{3}F_f\zeta G^*(\omega). \tag{6}$$

Equation (6) can be written as

$$K^*(\omega) = \lambda G^*(\omega), \tag{7}$$

where $\lambda = \frac{8}{3}F_f\zeta$ has unit of length and is used to relate the complex elastic constant with the complex shear modulus.

III. MATERIALS AND METHODS

A. Cell samples

Blood samples used in this study were provided by healthy adult volunteers. A written form of consent was issued to and collected from all volunteers. The procedures applied for collecting and subsequent use of samples were performed in accordance with a protocol previously approved by the Research Ethics Committee of the University Hospital Clementino Fraga Filho from the Universidade Federal do Rio de Janeiro (Permit No. 074/10). A diminutive drop of fresh blood was first collected from one finger of each volunteer. Next, a suspension of red blood cells was obtained by mixing 0.2 μL of whole blood with 500 μL of phosphate buffered saline (PBS) supplemented with 1 mg/mL bovine serum albumin (BSA), following a previously established protocol [26]. Then 150 μL of this suspension was placed inside a rubber ring, with a diameter of 10 mm and a thickness of 2 mm, preattached to a clean glass coverslip using silicone grease. After 5 to 10 min, the cells adhered weakly and nonspecifically to the glass substrate. The adhesion was characterized by a small area as seen in the bright-field [Fig. 4(a), black arrows] and scanning electron microscopy [Fig. 4(d), white arrows] images, pointing out the adhesion spots. Then, 0.2 μL of a (10% v/v) solution of polystyrene microspheres (Polysciences, Warrington, USA) of radius (1.52 ± 0.02) μm was added, and the sample was taken to the OT microscope.

B. Optical tweezers

The OT setup employed in this work was previously described [19,27]. Briefly, a linearly polarized laser beam (IPG Photonics, model YLR-5-1064LP) with wavelength of 1064 nm in TEM_{00} mode was directed to the back entrance of a PLAN APO 100 × 1.4 NA DIC H Nikon objective of an inverted microscope Nikon TI-S (Nikon, Melville, NY). The optical trap was calibrated using the Stokes method and the trap transverse stiffness κ per unit power at the objective entrance P_E was determined: $\kappa/P_E = (0.16 \pm 0.02)$ pN μm^{-1} mW^{-1}, giving $\kappa = (96 \pm 12)$ pN/μm for the laser power set in the experiments.

C. Red blood cell tether extraction

To extract a tether, an uncoated polystyrene microsphere of radius (1.52 ± 0.02) μm was captured using the OT, and then the sample was moved until the trapped sphere was placed over an RBC attached to the coverslip [see Fig. 4(a), mark 1].

The trapped bead was then pressed against the RBC surface for 5 s to allow bead attachment. The polystyrene beads were attached to the RBC surface by nonspecific adhesions which likely involves van der Waals forces. Previous studies from our group have shown the strong attachment of uncoated polystyrene beads to the surfaces of different cells [19,20,27–29]. Moreover, it was already demonstrated that bead coating and size do not seem to affect tether force measurements [20]. The coating only helps to induce a more efficient first contact between the bead and cell surface. The most important caution during the experiment was to properly press, by defocusing the sample, the OT-trapped-bead against the cell surface, increasing the optical force intensity when pressing the sphere against the cell surface. After that, the sample was displaced using a piezoelectric positioning system E710 (PI, Germany) at constant speed V_T. The sample movement induced a change in the equilibrium position of the trapped bead over time, and the RBC deformed until it reached a point where a thin membrane tube (tether) was formed [20]. Images of the entire process were recorded by a CMOS camera C11440-10C (Hamamatsu, Japan) at a frame rate of 25 Hz. Before attachment to the RBC, a movie of a trapped microsphere was also recorded in order to determine a position reference for zero force. To determine the microsphere center of mass in each frame of a tether extraction movie, the ImageJ software (National Institutes of Health, Bethesda, MD) was employed. Finally, by using the displacement of the microsphere in relation to the reference for zero force, and the trap calibration, the tether force was obtained. The data were analyzed using Kaleidagraph software (Synergy Software, USA). All the tether extraction experiments were performed at room temperature $(25 \pm 1)\,^{\circ}$C. For all tether pulling speeds, the sample was displaced by a fixed distance of 20 μm, resulting in tether lengths of about $\approx$10 μm.

D. Tether recoil

After pulling a tether with a length of 10 μm, the piezoelectric positioning system was stopped and the optical trap was turned off, releasing the microsphere, which moved toward the RBC as the tether length decreased, until the sphere touched the cell. A movie of the entire process was recorded, and the center-of-mass position (ρ_r) of the microsphere during tether recoil was determined as a function of time. The experiments were performed in four different RBCs and for two extraction pulling speeds, $V_T = 0.5$ and $V_T = 5.0$ μm/s. To determine the characteristic decay times on tether recoil experiments, we adjusted the curves of ρ_r for each condition with two added exponential functions with different decay times.

E. Scanning electron microscopy

The measurements of tether radius extracted from RBCs were performed following the same procedures described in Ref. [20]. Immediately after the tether extraction experiments, the beads used to extract the tethers were attached to the coverslip. The samples were then fixed with glutaraldehyde, 2.5%, in a 0.1M cacodylate buffer (pH = 7.4) for 40 min at room temperature, dehydrated in an ethanol series, critical-point-dried (BAL-TEC, Fuerstentum, Liechtenstein), mounted on specimen stubs, gold-sputtered (BAL-TEC), and observed in an EVO 40 scanning electron microscope (Carl Zeiss, Jena, Germany). After image acquisition and analysis, the tether radius value was obtained following the procedures described in Ref. [20], and using the analysis of the gray level profile in the direction perpendicular to the tether axis.

F. Confocal fluorescence microscopy

Immediately after tether pulling experiments with optical tweezers, the RBCs were fixed for 15 min with PBS-paraformaldehyde 4%, treated with PBS-triton X100 0.2% for 5 min, blocked with PBS-BSA 5% (Sigma-Aldrich, USA) for 30 min and incubated for 2 h with phalloidin-FITC (Sigma-Aldrich, USA). The sample was then moved to a TCS-SP5 II confocal microscope (Leica Microsystems, Germany). Confocal fluorescence images were captured employing LAS AF 2.2.0 software (Leica Microsystems). Confocal Z projection images in the XZ direction showing RBC cells stained for F-actin (using Phalloidin-FITC) were collected at every 0.3 μm also using the LAS AF 2.2.0 software (Leica Microsystems).

The fluorescence intensity (FI) associated the amount of F-actin inside the tether for tethers extracted from the surface of RBCs were measured. The fluorescence intensity values obtained were considered as the mean $\pm$ standard error of four different tethers. The fluorescence intensity inside the RBC cell ($\mathrm{FI}_{(\mathrm{cell})}$) was also measured. All values were normalized by $\mathrm{FI}_{(\mathrm{cell})}$.

G. Defocusing microscopy and form factor

In order to characterize the shape of deformed and undeformed RBCs, 5000 focused images and 5000 defocused images (2 μm) of the same cell were obtained at a capture rate 110 Hz, and averaged to give the results presented in Figs. 2(a), 2(b), 2(d), and 2(e). The deformed RBCs were obtained by extracting a tether and fixing the microsphere to the coverslip. The images were analyzed with ImageJ using defocusing microscopy to get the RBC height profiles presented in Figs. 2(c) and 2(f).

Following Ref. [18], the uncertainty associated with the axial position (Δz) can be estimated by

$$\Delta z = \frac{n_{ob}\Delta C_{\min}}{\Delta n \nabla^2 H(0)}, \tag{8}$$

where $n_{ob} = 1.5$ is the glass refractive index, $\Delta n = 0.06$ is the difference between the refractive index of the RBC and the medium, and $\nabla^2 H(0) = 1.7\ \mu\mathrm{m}^{-1}$ is the Laplacian of RBC height profile at the cell center. For the optical setup with a Hamamatsu camera employed in this work, $\Delta C_{\min} \approx 0.02$, so $\Delta z \approx 0.3$ μm.

A customized ImageJ macro together with Kaleidagraph were used to determine the form factor from the RBC height profiles.

H. Red blood cell microrheology

The RBC microrheology experiments were performed adapting the procedures previously described [19]. Briefly, two polystyrene microspheres of radius (1.52 ± 0.02) μm

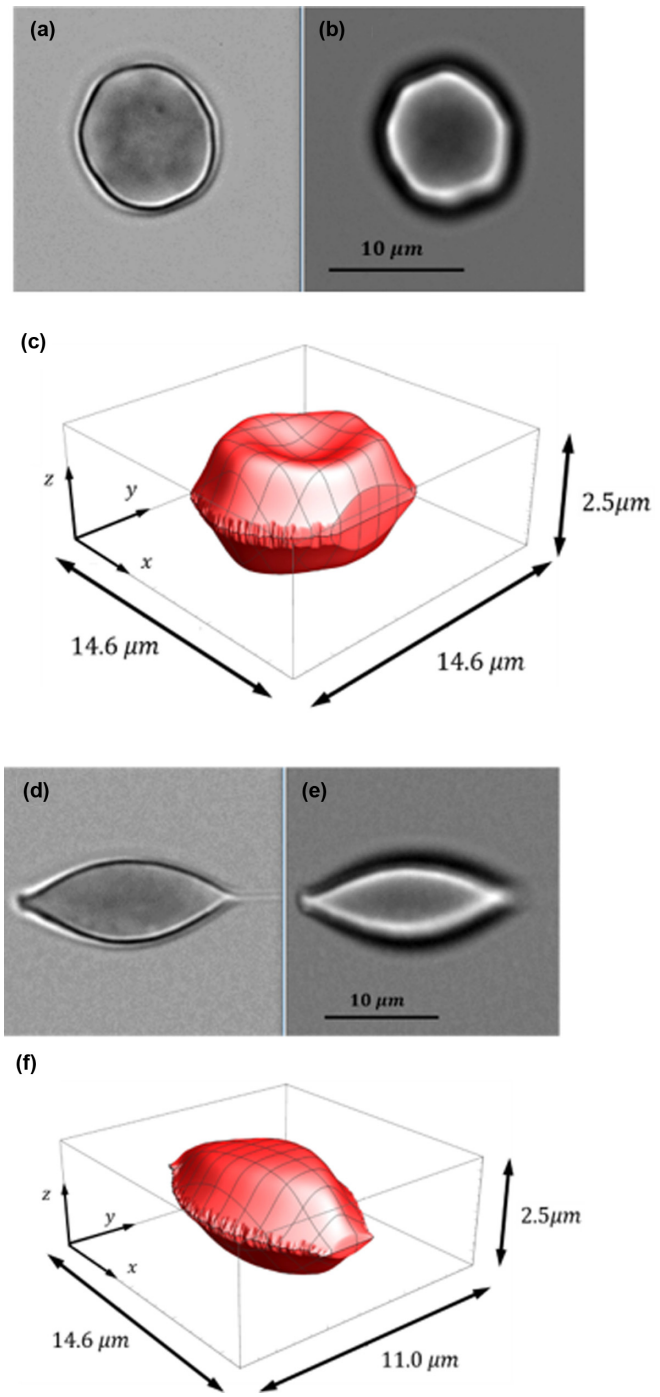

FIG. 2. Images for morphological characterization of RBC height and tether radius. [(a), (d)] In-focus images of nondeformed and deformed RBC, respectively. [(b), (e)] 2-μm defocused images of nondeformed and deformed RBC, respectively. [(c), (f)] 3D reconstruction of nondeformed and deformed RBC, respectively, obtained with defocusing microscopy.

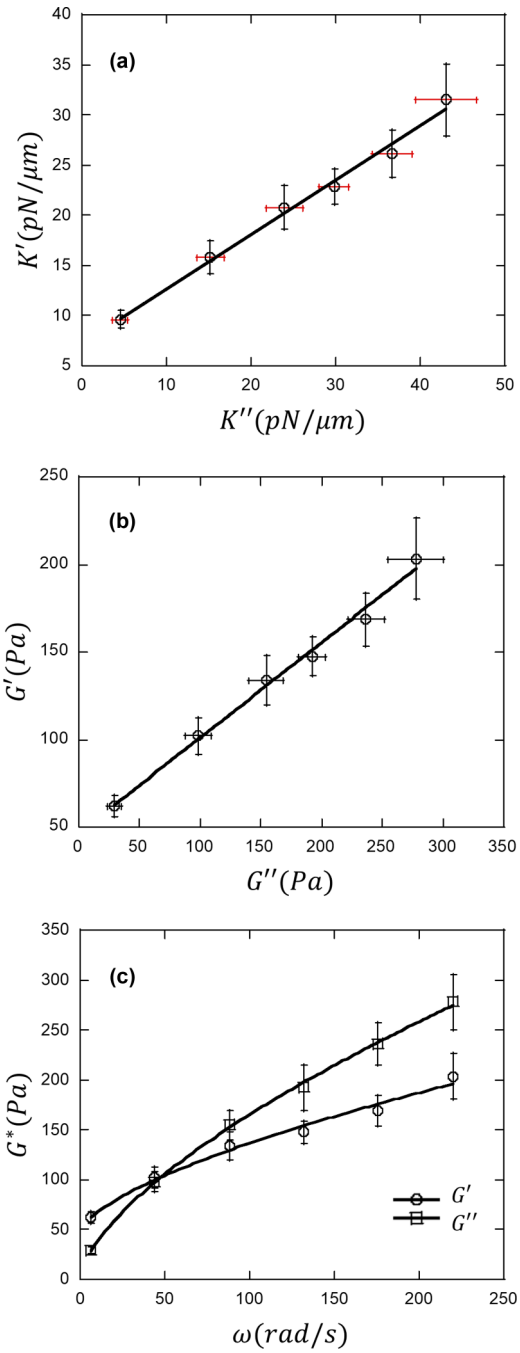

FIG. 3. RBC microrheology results. (a) Storage elastic constant (K') as a function of the loss elastic constant, K''. (b) Storage shear modulus (G') as a function of the loss shear modulus, G''. (c) Complex shear modulus $G^*(\omega)$ as a function of the angular frequency ω. Continuous lines in panels (a) and 9b) represent linear fits and in panel (c), fits to Eqs. (19) and (20); see text for details.

were used [19]. The first one was fixed to the coverslip, in a region near a chosen RBC, to be used as a position reference. The other microsphere was trapped and adhered to the chosen RBC surface. The cell was then stretched until its deformation reached the value for the situation described in Fig. 4(a), mark 2. In this situation, the cell had approximately the same form as that described in Fig. 4(b), after tether extraction. The sample was then subjected to a sequence of five cycles of harmonic oscillatory motions with amplitude $\xi_0 = (1.000 \pm 0.001)\,\mu$m. Each cycle had steps with the following linear frequencies f: 1, 7, 14, 21, 28, and 35 Hz. Images of the entire process were recorded using a Digital Hamamatsu C11440-10C camera with a capture rate of circa 790 Hz. The

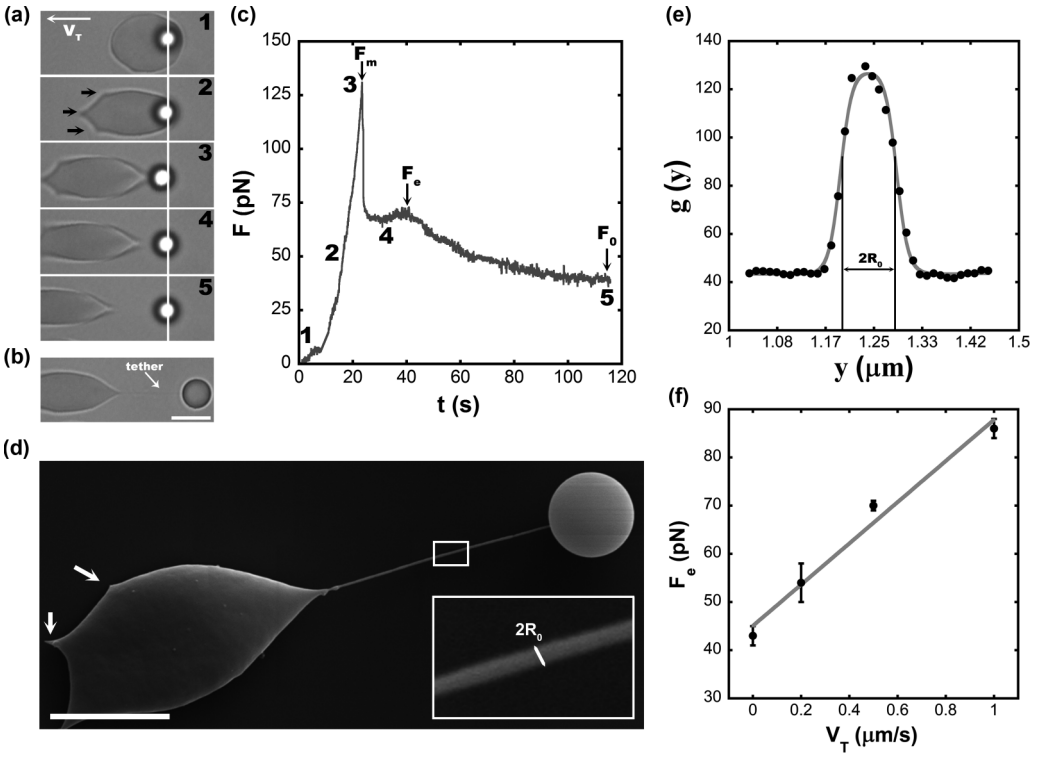

FIG. 4. Tether extraction experiment: (a) Sequence representing the increase in the cellular deformation as the sample moves (marks 1 to 3), the point in the extraction process where the force has its maximum value (mark 3), and the force plateau (mark 4) in the tether extraction. Black arrows indicate adhesion spots. (b) Tether image, scale bar 5 μm. (c) Force curve; see text for details. (d) SEM image of a tether used to measure the tether radius. White arrows indicate adhesion spots. Scale bar 5 μm. (e) Determination of the tether radius using the gray level profile obtained from the SEM image; see Ref. [20] for details. With the SEM image analysis the value of $R_0 = (46 \pm 2)$ nm was obtained. (f) Tether extraction force F_e as a function of the extraction pulling speed V_T.

ImageJ and Kaleidagraph programs were, respectively, used to analyze the images and data.

The position $\xi(t)$ of the reference microsphere follows the sample movement and is described by

$$\xi(t) = \xi_0 \cos(\omega t), \tag{9}$$

where $\omega = 2\pi f$ is the angular frequency. The position $\rho(t)$ of the microsphere attached to the RBC and trapped by the OT is given by [19]

$$\rho(t) = \xi_0 \cos(\omega t) - \xi' \cos(\omega t - \varphi), \tag{10}$$

where ξ' is the out of phase amplitude and φ is the out of phase angle. Both quantities are related to the RBC complex elastic constant $K^*(\omega) = K'(\omega) + iK''(\omega)$, as shown below:

$$K'(\omega) = \kappa(\xi_0/\xi')\cos(\varphi) - \kappa, \tag{11}$$

and

$$K''(\omega) = \kappa(\xi_0/\xi')\sin(\varphi) - \omega\beta, \tag{12}$$

where κ is the OT elastic constant and β is the Stokes-Faxén fluid friction coefficient [20] for the trapped microsphere at a distance $h = (2.5 \pm 0.5)$ μm of the coverslip. The value of h was evaluated by image analysis [19]. For each value of linear frequency f, and each condition tested, five measurements were performed. Values of K' and K'' were determined as the average results obtained using Eqs. (11) and (12) and the analysis of the reference and trapped microsphere positions. The error bars were considered as the standard errors of the means.

I. Red blood cell soft glassy rheology model

The soft glassy rheology model was developed by Sollich *et al.* to describe glassy materials such as emulsions, pastes, and slurries [30]. The model is based on two properties shared by these materials, metastability and structural disorder. The complex shear modulus of soft glassy materials is described by a power law dependency of the storage and loss moduli with frequency and a linear relation between them. It has been shown [31,32] that the soft glassy rheology model can be used to characterize the viscoelastic response of cells. A universal weak power law with exponent value $\approx$0.2 was observed for different types of adherent cells in a large range of frequencies. We propose that the model can also be used to describe RBC viscoelasticity.

The complex RBC elastic constant $K^*(\omega)$ [19] was measured as a function of the harmonic oscillatory stimulus of angular frequency ω. $K^*(\omega) = K'(\omega) + iK''(\omega)$ where $K'(\omega)$ is the storage elastic constant and $K''(\omega)$ is the loss elastic constant. $K^*(\omega)$ is related to the RBC complex shear modulus $G^*(\omega) = G'(\omega) + iG''(\omega)$ by Eq. (6), where F_f is a form factor that depends on the RBC geometry and ζ is the RBC membrane thickness. $G'(\omega)$ and $G''(\omega)$ are, respectively, the RBC shear storage and shear loss moduli.

The generalized Maxwell-Wiechert rheology model [33] was used to characterize the RBC membrane in this work. It is represented by an association of a spring, with constant shear modulus G_m, in parallel to an infinite number of Maxwell blocks (one spring associated in series with a dashpot), each one with a specific relaxation time. The association of Maxwell elements can be represented by a complex shear modulus $G^*_{SG}(\omega)$, that shows a power law dependence with angular frequency, this being a characteristic of soft glassy materials (SGM) [31]. The SGM storage modulus is given by

$$G'_{SG}(\omega) = G_0\left(\frac{\omega}{\omega_0}\right)^{\alpha}, \tag{13}$$

and the SGM loss modulus is written as

$$G''_{SG}(\omega) = G_0\tan(\delta)\left(\frac{\omega}{\omega_0}\right)^{\alpha}, \tag{14}$$

where G_0 is the low-frequency storage modulus, defined as the storage modulus at the frequency $\omega_0 = 1$ rad/s, $\tan(\delta)$ is the ratio G''_{SG}/G'_{SG} that is constant for SGM, and α $(0 < \alpha < 1)$ is a parameter that characterizes the material's viscoelastic response. $\alpha = 0$ means solid behavior and $\alpha = 1$ indicates liquid behavior [19,31].

For viscoelastic materials, besides the complex shear modulus, the complex shear viscosity $\eta^*(\omega)$ [34] can also be defined as

$$\eta^*(\omega) = [G^*(\omega)/(i\omega)]. \tag{15}$$

The complex viscosity $\eta(\omega)$ is given by the magnitude of the complex number that describes the complex shear viscosity:

$$\eta(\omega) = |\eta^*(\omega)| = \frac{1}{\omega}\sqrt{[G'(\omega)]^2 + [G''(\omega)]^2}. \tag{16}$$

For an SGM, $\eta_{SG}(\omega)$ is then written as

$$\eta_{SG}(\omega) = \eta_0\left(\frac{\omega}{\omega_0}\right)^{\alpha-1}, \tag{17}$$

where η_0 is a constant, given by

$$\eta_0 = (G_0/\omega_0)\sqrt{1 + \tan(\delta)^2}. \tag{18}$$

η_0 can be seen as the material viscosity at frequency ω_0. In all the analysis done in this work, we set $\omega_0 = 1$ rad/s. For this reason, η_0 is called the low-frequency viscosity of the material. In terms of α, G_0, G_m, and η_0 the storage and loss moduli of the RBC can then be written respectively as

$$G'(\omega) = G_m + G_0\left(\frac{\omega}{\omega_0}\right)^{\alpha} \tag{19}$$

and

$$G''(\omega) = G_0\left(\frac{\omega}{\omega_0}\right)^{\alpha}\sqrt{\left(\frac{\omega_0\eta_0}{G_0}\right)^2 - 1}. \tag{20}$$

IV. RESULTS

A. Red blood cell form factor

We measured the form factor of the deformed RBC by analyzing its height profile using defocusing microscopy, and 3D representations of nondeformed and deformed erythrocytes are presented in Figs. 2(a)–2(f). For the deformed condition, we found $F_f = (0.64 \pm 0.02)$ after the analysis of ten images with the standard error of the mean considered as the error bar. For the nondeformed condition, the same procedure was applied to fifteen images, and we found the value (1.28 ± 0.01) for the form factor in this case. This result indicates that a factor of about 2 in the values of the RBC storage and loss shear moduli could be observed if the F_f parameter is not properly considered. The RBC membrane thickness can be determined by adding the reported value for RBC cortical cytoskeleton thickness (82 ± 8) nm [6] to the phospholipid bilayer thickness 5 nm, giving $\zeta = (87 \pm 8)$ nm. We found for the deformed RBC $\lambda_d = (0.15 \pm 0.01)$ μm, and so $K^*(\omega) = [(0.15 \pm 0.01)\ \mu\text{m}]G^*(\omega)$.

B. Red blood cell microrheology

Figure 3(a) shows the storage elastic constant as a function of the loss elastic constant obtained by the RBC microrheology experiments. The complex elastic constant associates forces with deformations (elastic response) and speeds (loss response). To obtain the relationship between stresses and strains, the cell morphology must be considered. Using defocusing microscopy and the form factor definition, we found $K^*(\omega) = [(0.15 \pm 0.01)\ \mu\text{m}]G^*(\omega)$, and the complex shear modulus was determined from the measured complex elastic constant. The results are presented in Fig, 3.

From the linear fit shown in Fig. 3(b), the value of $G_m = (49 \pm 5)$ Pa was found. After fixing this value in the $G'(\omega)$ fit to Eq. (19), the values of $G_0 = (5 \pm 1)$ Pa and $\alpha = (0.65 \pm 0.06)$ were obtained. Finally, after using the result for G_0 obtained from the fit to Eq. (19), and fixing it in the $G''(\omega)$ fit to Eq. (20), $\eta_0 = (9.9 \pm 0.6)$ Pa s and $\alpha = (0.64 \pm 0.02)$ were determined [Fig. 3(c)]. The method of least squares was used to get the average values and respective uncertainties from the data. The linear dependency of $G'(\omega)$ with $G''(\omega)$ agrees with the hypothesis that the RBC membrane can be modeled as a SGM. Besides, the average value for α, $\bar{\alpha} = 0.65 \pm 0.03$, indicates that the RBC membrane is a viscoelastic material with a liquid-like behavior.

The soft glassy behavior was previously observed in the elastic response of adherent cells [31]. In that case, the power law coefficient describing the complex shear modulus has a value near 0.2, indicating a solid-like behavior. The RBC by its turn is a very peculiar cell, since it does not have a nucleus and its role in the human body demands that it must flow with blood. A power law in the frequency, for the viscoelastic response of RBCs, with a value near 0.6, was also previously observed, without any mention of the soft glassy model [17]. The soft glassy phenomenological model in this study indicates that RBCs, when deformed, present a liquid-like behavior, a signature of the peculiar mechanical properties of these cells. This feature is used by the RBCs to allow them to pass through the narrowest capillaries of the blood circulatory system.

C. Tether extraction experiments

Figures 4(a)–4(c) present a typical result of a tether extraction experiment performed in a healthy RBC placed in

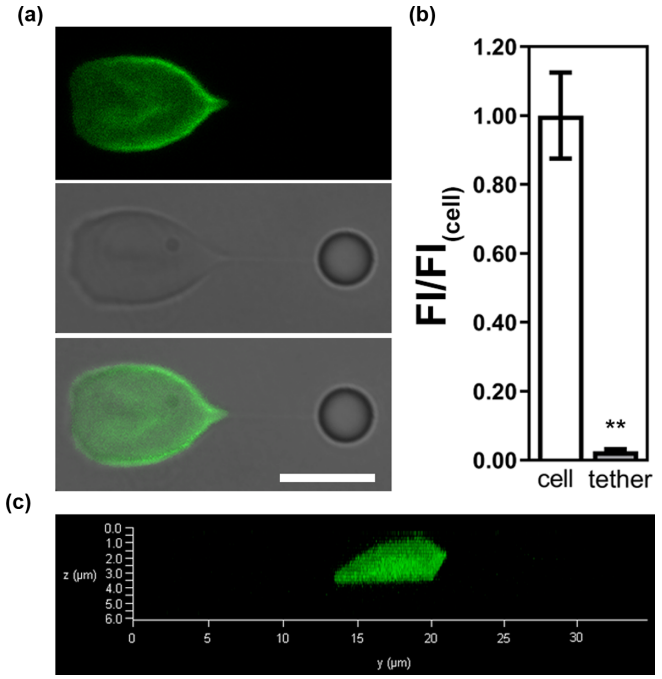

FIG. 5. Images of tethers extracted from RBCs do not present F-actin staining. (a) (1) Confocal image of an RBC cell stained for F-actin (phalloidin-FITC), (2) bright-field image of the RBC cell presented in (1), a membrane tether is observed between the RBC surface and the bead, (3) bright-field/fluorescence merge image showing that the tether extracted from RBC does not present F-actin staining. Scale bar is 5 μm. (b) Plot representing the fluorescence intensity (FI) of cell and tether, normalized by the mean fluorescence intensity inside the cell ($FI_{(cell)}$). Standard errors were used as error bars. Four different tethers extracted from different RBC cells were used for quantification ($**$ means $p < 0.01$ in t-test statistics, when comparing cell and tether experimental conditions). (c) Confocal Z projection image in the XZ direction showing the RBC cell stained for F-actin. Z-stack images were collected at every 0.3 μm.

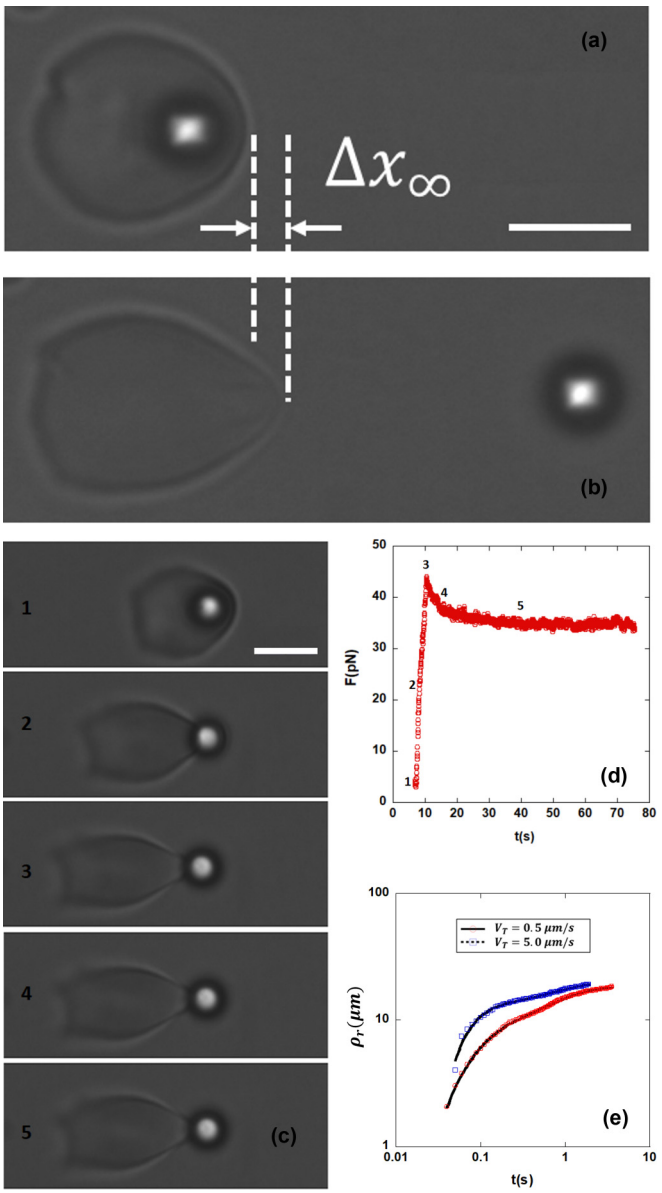

FIG. 6. (a) Nondeformed RBC attached to a microsphere. (b) Deformed RBC after tether formation when the force reaches the equilibrium value F_0; Δx_∞ is the cell deformation for this situation. Scale bar 5 μm. [(c), (d)] Force relaxation observed in an RBC before tether formation. Marks on panel (c) (scale bar 5 μm) are related with time instants and respective force values in panel (d). The sample was stopped before tether formation at instant $t \sim 12$ s (mark 3). A force relaxation process with a decay time $\approx$15 s, without visible changes in the cell morphology, is observed. (e) Typical result of a tether recoil experiment. Two conditions are represented, after pulling a tether with $V_T = 0.5$ μm/s (circles) and $V_T = 5.0$ μm/s (squares). For the tether pulling speed of 0.5 μm/s, the decay times $\tau_1 = (0.092 \pm 0.007)$ s and $\tau_2 = (1.4 \pm 0.4)$ s are determined. For the tether pulling speed of 5.0 μm/s, the decay times $\tau_1 = (0.06 \pm 0.01)$ s and $\tau_2 = (0.6 \pm 0.2)$ s are obtained.

an isotonic medium. When the sample started to move the cell, was deformed and the microsphere equilibrium position in the OT (marks 1, 2, and 3) changed, applying a force of intensity F in the cell-bead contact area. As the cell deformation increased with time t, the RBC applied force also increased until a maximum value F_m. After that, a membrane tether was formed and the force to increase the tube length, the extraction force F_e, remained constant during extraction (mark 4). In the case of Fig. 4(c), the tether pulling speed was 0.5 μm/s. For $t = t_e = 40$ s, the sample stage was stopped, and a relaxation process in the force was observed. This process is characterized by a relaxation time τ that depends on the tether extraction experimental conditions. The tether force value F_0 was determined by the asymptotic value of force in the limit when time goes to infinity (mark 5).

1. Viscoelastic parameters

We defined the cell elastic constant when the system reaches equilibrium (k_∞) as the tether force divided by the cell deformation Δx_∞, measured with image analysis [Figs. 6(a) and 6(b)], so

$$k_\infty = \frac{F_0}{\Delta x_\infty}. \tag{21}$$

TABLE I. Tether extraction results obtained for different tether pulling speeds.

V_T (μm/s)	F_m (pN)	F_e (pN)	F_0 (pN)	σ (pN/μm)	B ($pN\mu$m)	τ (s)
0.2 ($n = 6$)	100 ± 10	53 ± 4	36 ± 3	62 ± 6	0.26 ± 0.02	45 ± 4
0.5 ($n = 6$)	110 ± 10	69 ± 1	44 ± 5	76 ± 9	0.32 ± 0.04	27 ± 3
1.0 ($n = 20$)	123 ± 6	83 ± 2	47 ± 2	81 ± 5	0.34 ± 0.02	18 ± 2

We found $k_\infty = (10.3 \pm 0.5)$ pN/μm, averaging results for all the tether extractions performed. Considering the RBC form factor measured for the deformed condition, a shear modulus $G_\infty = (69 \pm 6)$ Pa was obtained.

In a similar way, we defined the large deformation elastic constant $k_{\max}$ as

$$k_{\max} = \frac{F_m}{\Delta x_{\max}}, \tag{22}$$

where $\Delta x_{\max}$ is the maximum deformation applied to the RBC before tether formation. We found that $k_{\max}$ did not change with V_T and had value $k_{\max} = (25 \pm 1)$ pN/μm, averaging results for all the tether extractions performed and considering all pulling speeds used. Figure 4(a) indicates that the RBC morphology did not change appreciably when we compare the equilibrium and large deformation conditions. This observation suggests that the difference between $k_{\max}$ and k_∞ is related to membrane-cytoskeleton stiffening for large deformations [35]. Besides, considering the RBC form factor measured for the deformed condition, a shear modulus $G_{\max} = (167 \pm 13)$ Pa was obtained.

Hochmuth *et al.* [13] postulated three dissipative processes responsible for energy dissipation during tether extraction. These processes are characterized by three surface viscosity parameters related to the friction of the external RBC membrane monolayer and the external medium, the friction of the internal RBC monolayer with the RBC cytoskeleton, and the friction between the two RBC membrane monolayers. The combination of all these processes is represented by an effective surface viscosity parameter η_{eff} that relates the extraction force F_e, the extraction pulling speed V_T, and the tether force F_0 by

$$F_e = F_0 + 2\pi\eta_{\text{eff}} V_T. \tag{23}$$

Figure 4(f) shows the linear fit of the values presented in Table I using Eq. (23). We found $\eta_{\text{eff}} = (6.0 \pm 0.6)$ pN μm^{-1} s.

The decay time τ was obtained by adjusting the decay process in the tether force with the equation

$$F(t') = (F_e - F_0)e^{-t'/\tau} + F_0, \tag{24}$$

where $t' = t - t_e$, and t_e is the value of time when the tether extraction is interrupted: $F(t_e) = F_e$ (see Fig. 4).

The force decay after stopping the sample movement in the tether extraction experiment indicates that a dissipative process with a decay time $\tau \approx 30$ s is taking place. To investigate if the relaxation process described in Fig. 4 was related to the tether or to the whole RBC, we used OT to deform an RBC with an amplitude similar to the one described in mark 2 of Fig. 4, and measured the force acting on the cell. As can be seen in Figs. 6(c) and 6(d), a force relaxation process with a characteristic timescale of the same order of τ was observed, although the cell deformation remained fixed. We assign this relaxation with an RBC membrane-cytoskeleton rearrangement not directly related to the cell deformation.

2. Elastic parameters for the lipid bilayer

The bending modulus B of the RBC membrane is given by [20,36]

$$B = \frac{F_0 R_0}{2\pi}, \tag{25}$$

and the surface tension σ of the RBC membrane is

$$\sigma = \frac{F_0}{4\pi R_0}, \tag{26}$$

where R_0 is the tether radius. To determine σ and B, we measured F_0 with OT-tether extraction and R_0 with scanning electron microscopy. Figure 4(d) shows a scanning electron microscopy (SEM) image of a tether extracted from a healthy RBC. The value of tether radius was determined using the SEM image, from the analysis of the gray level profile [Fig. 4(e)] in a direction perpendicular to the tether axis [20]. We found $R_0 = (46 \pm 2)$ nm, where the error bar was determined by the standard error of the mean obtained from 20 different tether SEM images. The SEM image also shows that the tether radius can be considered constant over the tether length. The analysis of the gray level profile perpendicular to the tether length for two different positions, 1 μm from the cell surface and 1 μm from the bead surface, showed a difference of only 5%. Results for the RBC tether extraction experiments using three different pulling speeds are presented in Table I.

Using confocal microscopy, we investigated actin localization inside RBC extracted tethers. Figure 5 shows that we were not able to detect F-actin in the tethers based on quantitative analysis of their fluorescence intensities, unlike that previously observed for fibroblasts [20] and central nervous system cells [28]. However, the surface tension and bending modulus values of the RBC membrane are like those of adherent cells [20,28]. Besides, for the RBC, σ and B values increased significantly when comparing results for tether pulling speeds of 0.2 and 1 μm/s (Table I).

V. DISCUSSION

This work has begun to establish a precise methodology to measure the RBC mechanical properties for future applications in *Plasmodium falciparum*–parasitized erythrocytes. We chose OT- based microrheology and tether extraction experiments to characterize the viscoelastic properties of the RBC membrane (lipid bilayer associated with cortical cytoskeleton), its lipid bilayer surface tension, and bending modulus. References in literature point to some discrepancies in the

RBC rheology that may be partially attributed to changes in the cell morphology. Here we characterized the RBC form factor using the well-established and noninvasive defocusing microscopy technique [21,23,24], as a possible way to clarify these reported differences. The complex shear modulus that characterizes the composite membrane can be obtained only if the geometry is considered [19] and to the best of our knowledge this was not properly performed before for RBC microrheology and tether extraction experiments.

Two methodologies were used to characterize the viscoelastic properties of the RBC membrane, one applying small cell deformations (microrheology) and another imposing large cell deformations (tether extraction experiments). With microrheology, cell deformations between 0.1 to 0.4 μm were imposed as the linear frequency of the sample displacement varied from 1 to 35 Hz. The cell length along the direction of deformation was $\approx$15 μm [see Fig. 2(f)]. We estimated that for this case the applied RBC strains ranged from 0.7% to 2.7%. On the other hand, during tether extraction experiments, we conjecture that there was a detachment of the phospholipid bilayer from the cortical cytoskeleton, and the RBC was submitted to a stretching procedure that imposed strains of the order of 50% (see Figs. 2 and 4), far from what should be expected for a linear elastic response. However, after tether formation the RBC strain was kept almost constant and only one characteristic relaxation time was observed [see Fig. 4(c)].

The low-frequency ($\omega \sim 1$ rad/s) RBC surface shear modulus obtained with microrheology measurements can be written as $\mu = (G_m + G_0)\zeta = (54 \pm 5)$ pN/μm^2 $\times$ (0.087 ± 0.008) μm, $\mu = (4.7 \pm 0.6)$ pN/μm. This value is in agreement with those for the RBC surface shear modulus reported in the literature [9], [10]. Whereas for tether extraction experiments, two surface shear moduli can be defined, $\mu_\infty = G_\infty \xi = (69 \pm 6)$ pN/μm^2 $\times$ (0.087 ± 0.008) μm, $\mu_\infty = (6.0 \pm 0.8)$ pN/μm, and $\mu_{\max} = G_{\max}\xi = (167 \pm 13)$ pN/μm^2 $\times$ (0.087 ± 0.008) μm, $\mu_{\max} = (15 \pm 2)$ pN/μm. Considering the error bars, μ and μ_∞ are not significantly different. We also observe that $\mu_{\max}$ is more than twofold higher than μ. Since we did not observe changes in cell morphology after stretching the cell in the range of deformations used to define $\mu_{\max}$, we conclude that the RBC membrane stiffens with increasing cell deformation, also in agreement with reported results [35].

With microrheology and tether extraction experiments, two different surface viscosity parameters can be defined. One is the low-frequency surface viscosity of the RBC membrane complex which is given by $\eta_{S0} = \eta_0\zeta = (9.9 \pm 0.6)$ Pa s $\times$ (0.087 ± 0.008) μm, $\eta_{S0} = (0.9 \pm 0.1)$ pNμm^{-1} s. The value found is also in agreement with other reported results obtained from different experimental approaches [12,14]. The characteristic timescale defined by $\tau_0 = \eta_{S0}/\mu = (0.19 \pm 0.03)$ s gives the well-characterized [37] RBC shape recovery relaxation time. On the other hand, tether extraction experiments allowed us to obtain $\eta_{\text{eff}} = (6.0 \pm 0.6)$ pN μm^{-1} s, which is one order of magnitude greater than η_{S0}. This difference is attributed [13,38] to the phospholipid bilayer detachment that occurs when the tether is formed. The characteristic timescale defined by large deformations can be written as $\tau_{\max} = \eta_{\text{eff}}/\mu_{\max} = (0.40 \pm 0.06)$. Although $\tau_{\max}$ and τ_0 are significantly different, $\tau_{\max}$ is also in the range of the RBC shape recovery relaxation time.

The values for decay time measured in our tether extraction experiments ($18\,\text{s} < \tau < 45\,\text{s}$) are one order of magnitude larger than τ_0 and $\tau_{\max}$, and out of the range of most reported results in the literature (0.1–0.3 s) [37]. A decay time of about $\approx$10 s was also observed in hydrodynamic deformation experiments in which cells were submitted to large strains after passing through engineered microchannels [37]. This slow relaxation was associated with rotation of the cell after a much faster shape recovery with a characteristic time of $\approx$0.3 s. However, this does not seem to be the mechanism responsible for the results, since in our experiments the RBCs are attached to the substrate. A decay time of $\approx$50 s was also observed after stopping tether pulling from outer hair cells [38], although the authors did not mention any possible mechanism that could be responsible for it. A decay time of $\approx$10 s was observed after stopping tether pulling from HEK293 cell lineage [39], and it was related to the tether radius relaxation wherein the membrane components flow from the cell into the tether, in response to a tension gradient induced by the tether force [40]. We also performed tether recoil experiments [see Fig. 6(e)] after turning off the optical trap. We observed decay times of $\approx$1 s or less, in all cases. Moreover, a force relaxation of the entire cell in an experiment that was interrupted before tether formation, showed a decay time in the same order of magnitude of τ [Fig. 6(d)]. We conjecture that this process may be due to some cytoskeleton rearrangement that does not alter the cell shape in bright-field images, but the precise mechanism responsible for such a slow relaxation process in RBC tether extraction cannot be specified.

In addition, tether extraction experiments also provide information regarding lipid bilayer physical properties, such as the surface tension (σ) and bending modulus (B). These physical quantities may be useful when combined with the viscoelastic characterization of the RBC membrane, once σ and B are influenced by the interaction between the lipid bilayer and its underlying cytoskeleton [20].

The RBC membrane surface tension values obtained for the three tether pulling speed conditions described in Table I are within the range of values measured for adherent cells [28]. The bending modulus $\bar{B}$ of the RBC membrane was determined, after averaging the values found for the three tether pulling speed conditions described in Table I. We found $\bar{B} = (0.31 \pm 0.02)$ pN μm. The RBC bending modulus measured in this work was similar to the bending modulus of adherent cells [28].

The results for B and σ indicate that the cytoskeleton also influences the RBC membrane properties measured with tether extraction experiments. These results, as proposed in Ref. [28], must be considered as effective membrane parameters. They represent the coupling between the membrane and the cytoskeleton in a way that it is not possible to separate their contributions. However, unlike what was observed for adherent cells, we did not detect actin in RBC extracted tethers (Fig, 5). Other published studies have already indicated the absence of cytoskeletal proteins in tethers extracted from RBCs [41,42]. For instance, Berk and Hochmuth [41], using the fluorescence recovery after photobleaching (FRAP) technique, concluded that their results supported a "model of

the tether as a hollow cylinder of lipid bilayer." Waugh and Bauserman [42], using fluorescent labeling of tethered cells, concluded that "integral membrane proteins are excluded from the tether." The RBC membrane surface tension and bending modulus obtained in this study suggest that they are very responsive to the interaction between the lipid bilayer and the cortical cytoskeleton.

The bending modulus of the phospholipid bilayer, described by the polymer brush model, is given by $B_{\text{brush}} = (1/24)Y_{PL}\zeta_{PL}^3$ [4,43], where $\zeta_{PL} = 5$ nm and Y_{PL} are, respectively, the phospholipid bilayer thickness and its Young's modulus. Using our result for the bending modulus, $B \sim 0.3\ \text{pN}\,\mu\text{m}$, we estimated the Young's modulus of the RBC lipid bilayer as $Y_{PL} = (60 \pm 4)$ M Pa. This value is six orders of magnitude greater than the value of G_m measured by microrheology experiments. Even using the composite membrane thickness instead of the thickness of the phospholipid bilayer, we still found a Young's modulus two orders of magnitude greater than G_m. This indicates that during tether formation the bending of the RBC lipid bilayer is the dominant physical process. The tether formation requires much more energy than the deformation applied in microrheology experiments. For instance, the energy U_t [44] of a tether with length $L \approx 10\ \mu\text{m}$, a bending modulus $B \approx 0.3\ \text{pN} \times \mu\text{m}$, a surface tension $\sigma \approx 70\ \text{pN}/\mu\text{m}$ and radius $R_0 \approx 50$ nm, typical parameters extracted from the present study, is given by $U_t = 2\pi\sigma R_0 L + \frac{B\pi L}{R_0} \approx 400\ \text{pN}\,\mu\text{m}$. The energy in the microrheology experiments can be estimated by $U_m \approx 0.5 k_\infty \Delta x_{\text{rheology}}^2$. Using again typical values obtained in our experiments, $k_\infty \approx 10\ \text{pN}/\mu\text{m}$ and $\Delta x_{\text{rheology}} \approx 0.4\ \mu\text{m}$, we find $U_m \approx 0.8\ \text{pN}\,\mu\text{m}$. U_t is more than two orders of magnitude greater than U_m, indicating that different mechanical aspects are accessed with the two experiments.

VI. CONCLUSION

We developed and applied a new methodology based on defocusing microscopy to characterize the cell geometry, in order to evaluate the influence of the cell morphology in the viscoelastic properties of healthy human red blood cells. We used OT-based microrheology to characterize viscoelastic properties when the cell was subjected to small strains. We found that the RBC membrane rheology can be well described by a soft glassy model, with a power law dependence of the complex shear modulus with the load angular frequency. In addition to the power law exponent, the proposed phenomenological model is characterized by two shear moduli and a low-frequency viscosity. For small strains, the red blood cell membrane presents a liquid-like behavior, while adherent cells are solid-like. We also used OT-based tether extraction to characterize the viscoelastic properties when the cell was subjected to large strains. In this case, we measured two surface shear moduli and one surface viscosity parameter. All obtained shear and viscosity parameters defined demand information about the cell geometry to be correctly evaluated. A slow relaxation process of the tether force after stopping the tether pulling was observed. We associated this process with some cytoskeleton rearrangement that does not alter the cell shape, although the precise mechanism needs further investigation. We also determined the surface tension and bending modulus of the RBC membrane lipid component. We showed that F-actin was not detected inside tethers, although erythrocytes have membrane physical properties similar to those of adherent cells. We argue that to properly compare the viscoelastic properties of red blood cells in different situations, the task of cell geometry characterization must be accomplished. Together, the methodologies and procedures applied in this study would allow the erythrocyte community to better explore the mechanical behavior of red blood cells and may be useful to characterize erythrocyte viscoelasticity changes in several blood diseases.

ACKNOWLEDGMENTS

We acknowledge Professor Marcelo B. Ribeiro for a critical reading of the manuscript. We thank the Brazilian funding agencies National Council for Scientific and Technological Development (CNPq), the National Institute of Science and Technology Complex Fluids (INCT-FCx), the São Paulo Research Foundation (FAPESP), the Carlos Chagas Filho Foundation for Research Support of Rio de Janeiro (FAPERJ), and the Foundation for Research Support of Minas Gerais (FAPEMIG). This study was financed in part by the Coordination for the Improvement of Higher Education Personnel (CAPES).

[1] A. Alaarg, R. Schiffelers, W. W. van Solinge, and R. Van Wijk, Red blood cell vesiculation in hereditary hemolytic anemia, Front. Physiol. **4**, 365 (2013).

[2] S. Kapishnikov, L. Leiserowitz, Y. Yang, P. Cloetens, E. Pereiro, F. A. Ndonglack, K. Matuschewski, and J. Als-Nielsen, Biochemistry of malaria parasite infected red blood cells by x-ray microscopy, Sci. Rep. **7**, 802 (2017).

[3] B. Franke-Fayard, J. Fonager, A. Braks, S. M. Khan, and C. J. Janse, Sequestration and tissue accumulation of human malaria parasites: Can we learn anything from rodent models of malaria, PLoS Pathogens **6**, e1001032 (2010).

[4] D. Boal, *Mechanics of the Cell*, 1st ed. (Cambridge University Press, Cambridge, UK, 2002).

[5] G. Lenormand, S. Hénon, A. Richert, J. Siméon, and F. Gallet, Direct measurement of the area expansion and shear moduli of the human red blood cell membrane skeleton, Biophys. J. **81**, 43 (2001).

[6] A. Nans, N. Mohandas, and D. L. Stokes, Native ultrastructure of the red cell cytoskeleton by cryo-electron tomography, Biophys. J. **101**, 2341 (2011).

[7] J. T. Davies and E. K. Rideal, *Interfacial Phenomena*, 2nd ed. (Academic Press, New York, 1961).

[8] E. Evans, New membrane concept applied to the analysis of fluid shear- and micropipette-deformed red blood cells, Biophys. J. **13**, 941 (1973).

[9] E. Evans, Bending elastic modulus of red blood cell membrane derived from buckling instability in micropipet aspiration tests, Biophys. J. **43**, 27 (1983).

[10] R. Waugh and E. Evans, Thermoelasticity of red blood cell membrane, Biophys. J. **26**, 115 (1979).

[11] J. P. Hale, C. P. Winlove, and P. G. Petrov, Effect of hydroperoxides on red blood cell membrane mechanical properties, Biophys. J. **101**, 1921 (2011).

[12] X. Liu, Z. Y. Tang, Z. Zeng, X. Chen, W. J. Yao, Z. Y. Yan, Y. Shi, H. X. Shan, D. G. Sun, D. Q. He, and Z. Y. Wen, The measurement of shear modulus and membrane surface viscosity of RBC membrane with ektacytometry: A new technique, Math. Biosci. **209**, 190 (2007).

[13] F. Hochmuth, J. Shao, J. Dai, and M. Sheetz, Deformation and flow of membrane into tethers extracted from neuronal growth cones, Biophys. J. **70**, 358 (1996).

[14] G. B. Nash, C. S. Johnson, and H. J. Meiselman, Mechanical properties of oxygenated red blood cells in sickle cell (HBSS) disease, Blood **63**, 73 (1984).

[15] R. Hochmuth, P. Worthy, and E. Evans, Red cell extensional recovery and the determination of membrane viscosity, Biophys. J. **26**, 101 (1979).

[16] M. S. Amin, Y. Park, N. Lue, R. R. Dasari, K. Badizadegan, M. S. Feld, and G. Popescu, Microrheology of red blood cell membranes using dynamic scattering microscopy, Opt. Express **15**, 17001 (2007).

[17] M. Puig-de Morales-Marinkovic, K. T. Turner, J. P. Butler, J. J. Fredberg, and S. Suresh, Viscoelasticity of the human red blood cell, Am. J. Physiol.-Cell Physiol. **293**, C597 (2007).

[18] P. M. S. Roma, L. Siman, F. T. Amaral, U. Agero, and O. N. Mesquita, Total three-dimensional imaging of phase objects using defocusing microscopy: Application to red blood cells, Appl. Phys. Lett. **104**, 251107 (2014).

[19] Y. A. Ayala, B. Pontes, D. S. Ether, L. B. Pires, G. R. Araujo, S. Frases, L. F. Romão, M. Farina, V. Moura-Neto, N. B. Viana, and H. M. Nussenzveig, Rheological properties of cells measured by optical tweezers, BMC Biophys. **9**, 5 (2016).

[20] B. Pontes, N. Viana, L. Salgado, M. Farina, V. M. Neto, and H. Nussenzveig, Cell cytoskeleton and tether extraction, Biophys. J. **101**, 43 (2011).

[21] U. Agero, C. H. Monken, C. Ropert, R. T. Gazzinelli, and O. N. Mesquita, Cell surface fluctuations studied with defocusing microscopy, Phys. Rev. E **67**, 051904 (2003).

[22] U. Agero, L. Mesquita, B. Neves, R. Gazzinelli, and O. Mesquita, Defocusing microscopy, Microscopy Res. Tech. **65**, 159 (2004).

[23] L. G. Mesquita, U. Agero, and O. N. Mesquita, Defocusing microscopy: An approach for red blood cell optics, Appl. Phys. Lett. **88**, 133901 (2006).

[24] J. C. Neto, U. Agero, R. T. Gazzinelli, and O. N. Mesquita, Measuring optical and mechanical properties of a living cell with defocusing microscopy, Biophys. J. **91**, 1108 (2006).

[25] N. W. Tschoegl, *The Phenomenological Theory of Linear Viscoelastic Behavior*, 1st ed. (Spring-Verlag, Berlin, 1989).

[26] T. Betz, M. Lenz, J.-F. Joanny, and C. Sykes, ATP-dependent mechanics of red blood cells, Proc. Natl. Acad. Sci. U.S.A. **106**, 15320 (2009).

[27] Y. A. Ayala, B. Pontes, B. Hissa, A. C. M. Monteiro, M. Farina, V. Moura-Neto, N. B. Viana, and H. M. Nussenzveig, Effects of cytoskeletal drugs on actin cortex elasticity, Exp. Cell Res. **351**, 173 (2017).

[28] B. Pontes, Y. Ayala, A. C. C. Fonseca, L. F. Romão, R. F. Amaral, L. T. Salgado, F. R. Lima, M. Farina, N. B. Viana, and V. M.-N. H. M. Nussenzveig, Membrane elastic properties and cell function, PLoS One **8**, e67708 (2013).

[29] B. Hissa, B. Pontes, P. M. S. Roma, A. P. Alves, C. D. Rocha, T. M. Valverde, P. H. N. Aguiar, F. P. Almeida, A. J. Guimarães, C. Guatimosim *et al.*, Membrane cholesterol removal changes mechanical properties of cells and induces secretion of a specific pool of lysosomes, PLoS One **8**, e82988 (2013).

[30] P. Sollich, F. Lequeux, P. Hébraud, and M. E. Cates, Rheology of soft glassy materials, Phys. Rev. Lett. **78**, 2020 (1997).

[31] X. Trepat, L. Deng, S. S. An, D. Navajas, D. J. Tschumperlin, W. T. Gerthoffer, J. P. Butler, and J. J. Fredberg, Universal physical responses to stretch in the living cell, Nature (London) **447**, 592 (2007).

[32] M. Balland, N. Desprat, D. Icard, S. Féréol, A. Asnacios, J. Browaeys, S. Hénon, and F. Gallet, Power laws in microrheology experiments on living cells: Comparative analysis and modeling, Phys. Rev. E **74**, 021911 (2006).

[33] T. Klöppel and W. A. Wall, A novel two-layer, coupled finite element approach for modeling the nonlinear elastic and viscoelastic behavior of human erythrocytes, Biomech. Model. Mechanobiol. **10**, 445 (2011).

[34] T. G. Mason, Estimating the viscoelastic moduli of complex fluids using the generalized Stokes–Einstein equation, Rheol. Acta **39**, 371 (2000).

[35] D. A. Fedosov, B. Caswell, and G. E. Karniadakis, A multiscale red blood cell model with accurate mechanics, rheology, and dynamics, Biophys. J. **98**, 2215 (2010).

[36] W. Helfrich, Elastic properties of lipid bilayers: theory and possible experiments, Zeitschr. Naturforsch. C **28**, 693 (1973).

[37] S. Braumuller, L. Schmid, E. Sackmann, and T. Franke, Hydrodynamic deformation reveals two coupled modes/time scales of red blood cell relaxation, Soft Matter **8**, 11240 (2012).

[38] Z. Li, B. Anvari, M. Takashima, P. Brecht, J. H. Torres, and W. E. Brownell, Membrane tether formation from outer hair cells with optical tweezers, Biophys. J. **82**, 1386 (2002).

[39] N. Khatibzadeh, S. Gupta, B. Farrell, W. E. Brownell, and B. Anvari, Effects of cholesterol on nano-mechanical properties of the living cell plasma membrane, Soft Matter **8**, 8350 (2012).

[40] P. Dommersnes, O. Orwar, F. Brochard-Wyart, and J. Joanny, Marangoni transport in lipid nanotubes, EPL **70**, 271 (2005).

[41] D. A. Berk and R. M. Hochmuth, Lateral mobility of integral proteins in red blood cell tethers, Biophys. J. **61**, 9 (1992).

[42] R. E. Waugh and R. G. Bauserman, Physical measurements of bilayer-skeletal separation forces, Ann. Biomed. Eng. **23**, 308 (1995).

[43] W. Rawicz, K. C. Olbrich, T. McIntosh, D. Needham, and E. Evans, Effect of chain length and unsaturation on elasticity of lipid bilayers, Biophys. J. **79**, 328 (2000).

[44] T. R. Powers, G. Huber, and R. E. Goldstein, Fluid-membrane tethers: minimal surfaces and elastic boundary layers, Phys. Rev. E **65**, 041901 (2002).